Surface topography with PDI holography

L. B. Baath, S.K. Abu Dalou, and B.G.Rosén
Halmstad University
Halmstad, Sweden
Lars.Baath@set.hh.se

Abstract: This paper presents topographic measurements of metal surface with Point Diffraction Interferometer (PDI) technique. Interferogram of a surface is created and recorded with different phase offsets. These are then combined to create a phase offset map of the surface. We demonstrate the use with the presentation of our first surface topographic map,

1. INTRODUCTION

Optical interferometers have been used to image gas flows since the early decades of the last century. These were intensity interferometers in the form of Mach-Zender or Michelson instruments and thus sensitive to changes of path length of the order of half a wavelength only. It was not until the discovery of the lasers that the difference in phase of the two paths could be determined with any better resolution that π. Optical interferometers are since then frequently and abundantly used in laboratory work. Such an instrument must have an object beam, illuminating the object to be measured, and a reference beam which are combined at the observing frequency. This fundamental property requires that the two beam paths are mechanically stable during the observing time and that the laser light stays coherent over the difference in light travel time of the two paths. This does in general exclude the use of diode lasers since these have intrinsically short coherence lengths, and creates problems in industrial applications where chaotic sonic waves create noise within the interferometer.

The Photonics group at Halmstad University originates from radio astronomy where interferometry has been used for imaging for over 50 years. The original discovery of its use can be traced back to 1948 [Bolton and Stanley 1948] when it was discovered that the strong radio source Cygnus A showed interferometer fringes in a single antenna on the cliffs overlooking the ocean outside Sydney Australia. The fringes were the results of interference between the radio wave going directly into the antenna and the wave reflected in the water below and into the antenna.

Since then radio astronomy has developed elaborate techniques for interferometry. Data are sampled at sites distanced from 100 m to 5000 km from each other and then brought together to a special processor unit. The data

are then delayed so that the optical axis of the interferometer is pointing towards the radio source, and each combination of element, or antenna, pairs is cross correlated. Thereafter a focused image is calculated using a calibration technique where the phase fluctuation of the atmosphere is reduced. With radio interferometers it is therefore possible to make images which are completely diffraction limited in resolution. The resolution can be chosen to fit the physics one wants to study and range from 10-100 arcseconds for connected element interferometers to 50 micro-arcseconds at high frequencies and long baselines. Figure 1 below [Baath 1993] shows a composite of images of the quasar 3C446 obtained with a variety of interferometers. The square in each image represents the full extent of the next image in the composite, showing the potential of interferometer techniques in range of resolution.

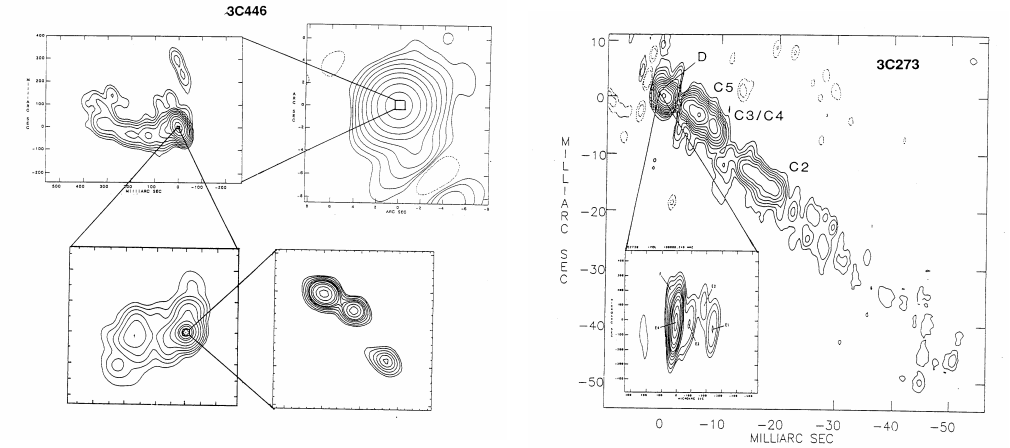

Figure 1 ; A composite of images of the quasar 3C446 (left panel) obtained with the VLA (top right), MERLIN (top left), cm VLBI (low left), and mm VLBI (low right); and the quasar 3C273 (right panel) observed with global VLBI at 6 cm and 3 mm (insert).

In Very Long Baseline Interferometry (VLBI) the elements are scattered over the world to synthesize an instrument which is equivalent to a radio telescope with the size of the globe. This is a very powerful tool for imaging and images with resolution better than 50 micro-arcseconds have been made. Figure 2 below shows a composite of images obtained at 6 cm [Zensus 1988] and 3 mm [Baath et al 1991] (insert) wavelengths of the quasar 3C273. The distinct “jet”-like feature and its curvature is typical for these types of cosmic radio sources and represents a power generator of some 10^{42} W [Baath 1991]. These machines are the most powerful in the universe and VLBI is the only instrument capable of making direct images of the close-in parts of these.

In radio astronomy, the objects are at large distances, some even at the very edge of the known Universe. They cannot be measured in any other way; the emission of light is intrinsic to the source; and it cannot be externally manipulated or determined. Experiments with the same type of observational instrument can be made in laboratory though, using smaller antenna arrays and

an external transmitter which is illuminating an object. We have made such observations at 3 cm wavelength, where an external transmitter illuminated the burden surface of a blast furnace. The reflected signal was received with a number of patch antennae. This procedure construed a interferometer array in two dimensions with an outside signal which was phase-locked to the receiver. The phase difference to between each antennae pair could thus be determined and the Z-axis could be determined by observing over a large number of narrow, mono-chromatic frequency channels. The resulting three dimensional surface reflections are shown in Figure 2 below [Nilsson, Baath and Malmberg 2007; Nilsson and Baath 2007].

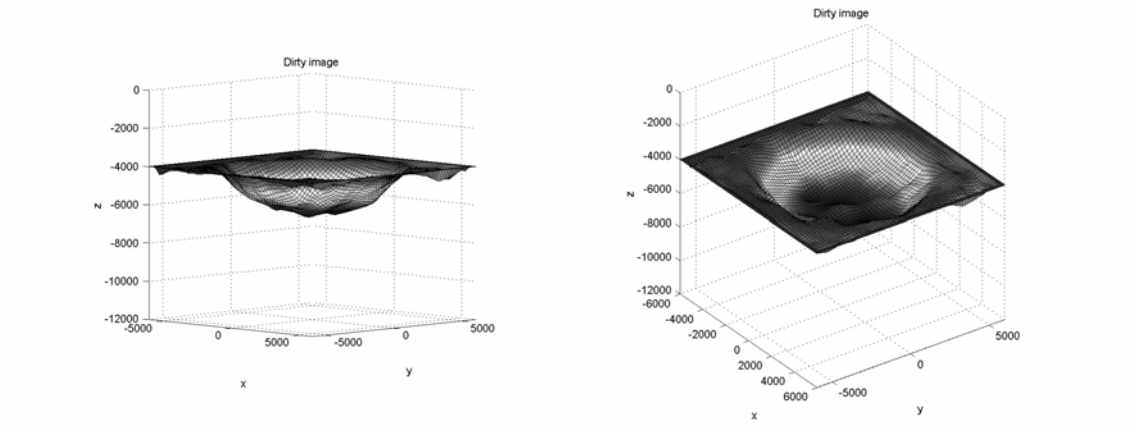

Figure 2 ; Three dimensional images of a blast furnace burden surface. Co-ordinates are in mm.

The principles to determine three dimensional images are the same for the radio, microwave and optical spectral bands. The ways and means differ in that the observational frequency can be mixed down to lower frequency while keeping phase in the radio and microwave bands, but not in the optical band. The data therefore have to be directly observed and the phase determined at the observational frequency in the optical. This makes the task more cumbersome, but the size of the array becomes smaller as the resolution scales with frequency, which makes optical interferometers more useful for objects smaller than a blast furnace.

2. PDI THEORY AND INSTRUMENTAL SET-UP

The *Point Diffraction Interferometer* (PDI) is especially designed to overcome the draw backs of the Mach Zender types of optical interferometer. The concept of PDI was developed in the 1970-ies [Smartt and Steel 1975] primarily for optical testing and then further developed to be used for flow visualization [Carr et al 1991]. The PDI concept has the object and reference beams going through the same optical path and thus eliminates the problem of short coherence

length, since the beams have nearly the same path lengths, as well as any noise from vibrations, since this will apply equally to both paths.

The PDI is essentially a common path interferometer. The mono-chromatic light from the target object is focused just shortly of a small area on a plate (Figure 3). The plate consist a semitransparent area, larger than the illuminated area, with a small pinhole in the center. The light wave front from the object passes attenuated through the area as the object beam. The pinhole creates its own spherical wave front with curvature radius as distance from the plate. The two wave fronts create an interference pattern which can be recorded with a CCD camera for further analysis. Typically the area has a transparency of about 2% and the pinhole is about 2.5 micrometers in diameter.

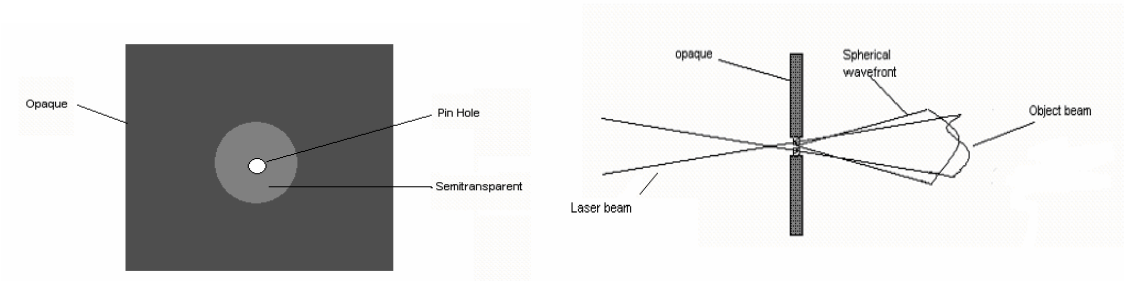

Figure 3 : Drawings showing the PDI pinhole geometry.

The PDI interferometer can be described analytically as follows. The co-oredinate system in the plane of the wave front is set to (x,y). r is the distance from the optical axis in the x,y plane, the diameter of test object is D and the diameter of the pinhole is d. λ is the observing wavelength, τ is the transperancy and W(x,y) is the phase at position (x,y) on the object wave front.

The complex amplitude of the object wave passing through the area is:

$$E_0(x,y) = e^{jkW(x,y)}.\mathrm{Cyl}(\frac{r}{D})$$

The amplitude transmittance of PDI plate is:

$$t(x,y) = \tau + (1-\tau)\mathrm{Cyl}(\frac{r}{d})$$

The resultant complex amplitude distribution at the camera image plane is the result of two wave fronts. The first is the attenuated object wave front passing through the semitransparent part of the PDI plate. The second is the convolution of the object wave front passing through the transparent part and the Fourier transform of the fully transparent pinhole transparent function:

$$E_i(x,y) = \tau \cdot \mathrm{Cyl}(\frac{r}{D}) e^{jkW(x,y)} + \left\{ \left[\mathrm{Cyl}(\frac{r}{D}) e^{jkW(x,y)} \right] \otimes \left[(1-\tau)\frac{\pi}{2} (\frac{r.d}{\lambda.f_2})^2 \right] \frac{J_1(\frac{\pi.r.d}{\lambda.f_2})}{(\frac{\pi.r.d}{\lambda.f_2})} \right\}$$

f_2 is the focal length of the focusing lens. J_1 is the first order Bessel function from the Fraunhofer diffraction of the circular pinhole aperture. The last factor of the equation is a Sombrero function and can be approximated to 1 near the pinhole. The resulting complex amplitude at the camera aperture is therefore:

$$E_i(x,y) = \tau \cdot \mathrm{Cyl}(\frac{r}{D}) e^{jkW(x,y)} + \left\{ \left[\mathrm{Cyl}(\frac{r}{D}) e^{jkW(x,y)} \right] \otimes \left[(1-\tau)\frac{\pi}{2} (\frac{r \cdot d}{\lambda \cdot f_2})^2 \right] \right\}$$

Assuming a constant phase over the pinhole and restricting the view to the beam area we can write the intensity variation across the camera aperture as:

$$I_0(x,y) = \left[E_i \cdot E^*{}_i \right] = (\tau)^2 + \left((1-\tau)\frac{\pi}{2} \left(\frac{d \cdot r}{\lambda \cdot f_2} \right)^2 \right)^2 + 2 \cdot \tau \cdot (1-\tau)\frac{\pi}{2} \left(\frac{d \cdot r}{\lambda \cdot f_2} \right)^2 \cdot \cos\varphi(x,y)$$

φ is the phase difference between the object wave front and the reference wave front. This equation represents the superposition of three images: the first term is the attenuated image of the object; the second term is the image of the pinhole wave front, or the pinhole point spread function; the third term is the cross-correlation between the two wave fronts and includes the differential phase distribution across the object field. Figure 4 below shows examples of PDI images taken across gas flows (Baath 2003).

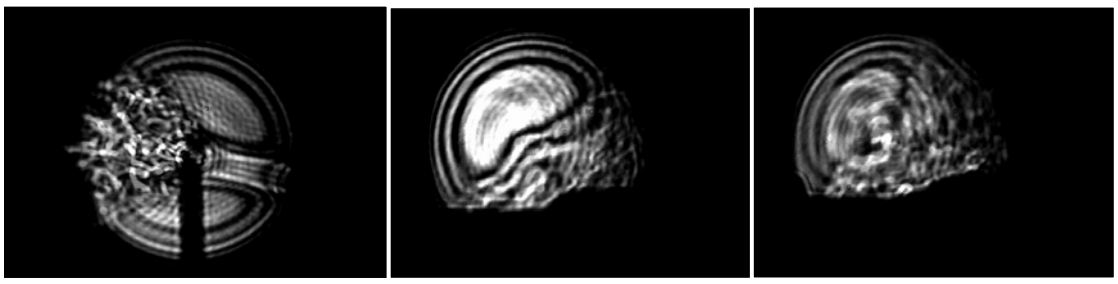

Figure 4 : PDI observations of gas flows. Left panel shows a laminar flow disturbed by an obstacle in its path. The flow is from right to left. The three overlaying images can clearly be seen. Middel and right panels show the flow of gas at the outlet of a flute. The cut in the flute can be seen at the bottom of the pictures. The flows show an F (middle) and a G (right)..

The phase information can be extracted by taking three images with the pinhole moved along the optical axis by ±λ/2. The phase can then be retrieved modulus two pi. The depth is the half path length since the object wave front is traveling double length when reflected from the surface and can be calculated with modulus one half wave length as:

$$\Delta l = \frac{1}{2} \cdot \frac{\lambda}{2\pi} \cdot \arctan\left[\frac{I_{-\frac{\lambda}{2}} - I_{+\frac{\lambda}{2}}}{2 \cdot I_0 - I_{+\frac{\lambda}{2}} - I_{-\frac{\lambda}{2}}} \right]$$

We have modified our experimental set-up to observe the three dimensional surface structure of reflecting objects. The modification implies reflecting the object beam at the surface rather than beam it through the gas flow. The experimental set-up is shown in Figure 5 below. The light from a laser is expanded to a suitable beam diameter. The beam is then reflected in a beam splitter prism to illuminate a metal object. The beam reflects off the object, passes through the beam splitter and is focused on the PDI pinhole area. A camera is then mounted in the combined path of the object and pinhole wave fronts. Three images are then recorded with the pinhole moved along the optical axis by ±λ/2 as previously discussed. The resulting interferogram represents the topographic map of the surface modulus one wavelength. Further ambiguity distance can be achieved by tracking the phase or, preferably, by observing at multiple wavelengths. Note that Speckle interferences are practically exterminated since these are coherent intensity patterns in the object beam and thus will be subtracted away as common to all three images.

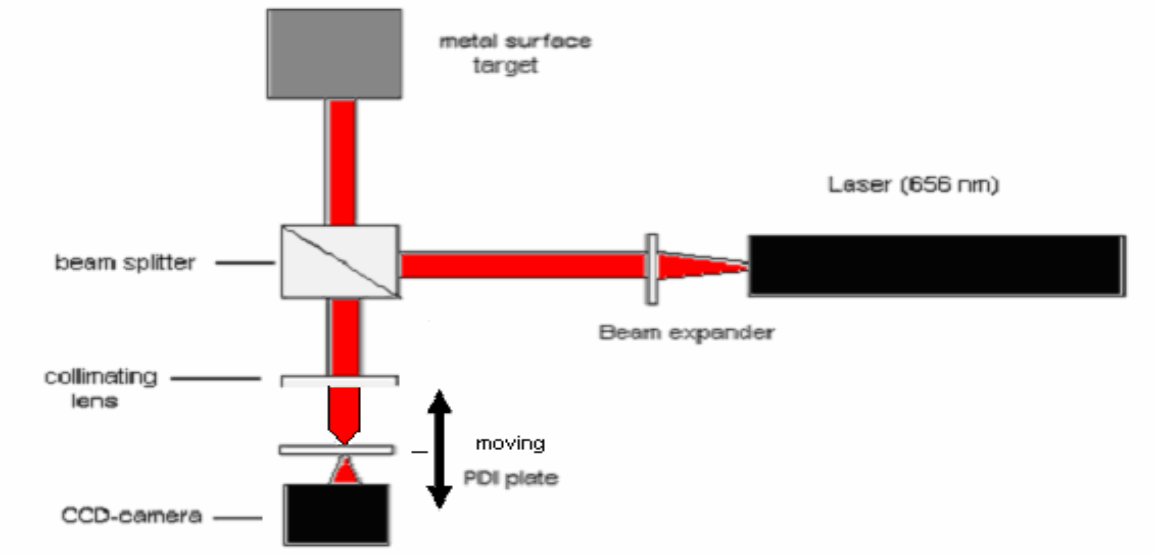

Figure 5 : PDI experimental set-up to observe the three dimensional surface structure of reflecting objects.

The resolution of the PDI system is limited in the plane of the surface by the number of pixels available on the CCD camera chip over the area of the illuminated surface. The observing time can be as short as milliseconds per image and a large area can therefore be covered in a second with multiple images with the object positioned at different positions. If a high density camera chip is used and the object is mounted on a moving platform, then a substantial area can be covered at high resolution in limited time. The resolution in depth (along the optical axis) is mainly limited by the grey scale resolution of the camera. At least 12 bits resolution is necessary to achieve resolution to 1% of a wavelength, or 12 nanometers (note that the light wave is reflected and therefore travels the offset distance twice) at red laser light. The depth resolution can be made better with higher grey scale resolution.

The ambiguity in distance is set by the wavelength, and can be extended by using multiple wavelengths. With two wavelengths λ_1 and λ_2 the ambiguity is:

$$ambiguity = \frac{1}{2} \cdot \frac{1}{\frac{1}{\lambda_1} - \frac{1}{\lambda_2}}$$

The ambiguity thus becomes 12 micrometers when combining the two wavelengths 635 and 670 nanometers.

3. RESULTS

In the following, we present results from our first experiments with PDI imaging. The surface we have chosen is a polished steel surface. Our selection was based on the principles to start with a rather smooth surface in order to eliminate too much phase winding across the observing field and to ensure a large reflection co-efficient.

Figure 6 shows our first PDI image of the selected object surface. The three overlapping intensity images from the pinhole, the surface and the interference pattern are obvious. The resolution of the camera is 12 bits in grey scale with 1220x1660 pixels. The laser light is from a Helium-Neon laser at 635 nanometers. The area covered by the camera chip is 500x700 micrometers on the metal surface.

Figure 7 shows the interferogram resulting from the three images with the pinhole translated a quarter of a wavelength backwards and forwards along the optical axis. The interferogram is dominated by a phase rotation caused by the curvature of the original laser wave front. The laser beam is not perfectly flat at the point of impact on the metal surface, and the resulting curvature is equivalent with a curved reflecting surface. A trough in the surface is indicated with an arrow in the figure. This trough is certainly a real feature as it is evident also in other sets of images taken with different illumination patterns and at various amplifications.

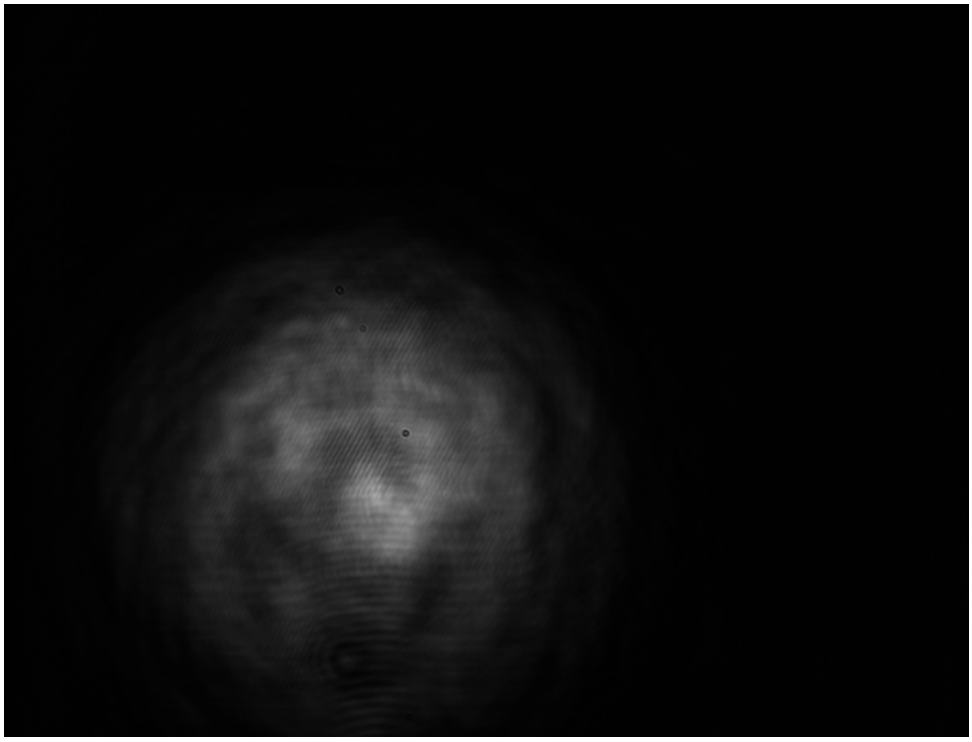

Figure 6 : PDI image of a polsihed steel surface.

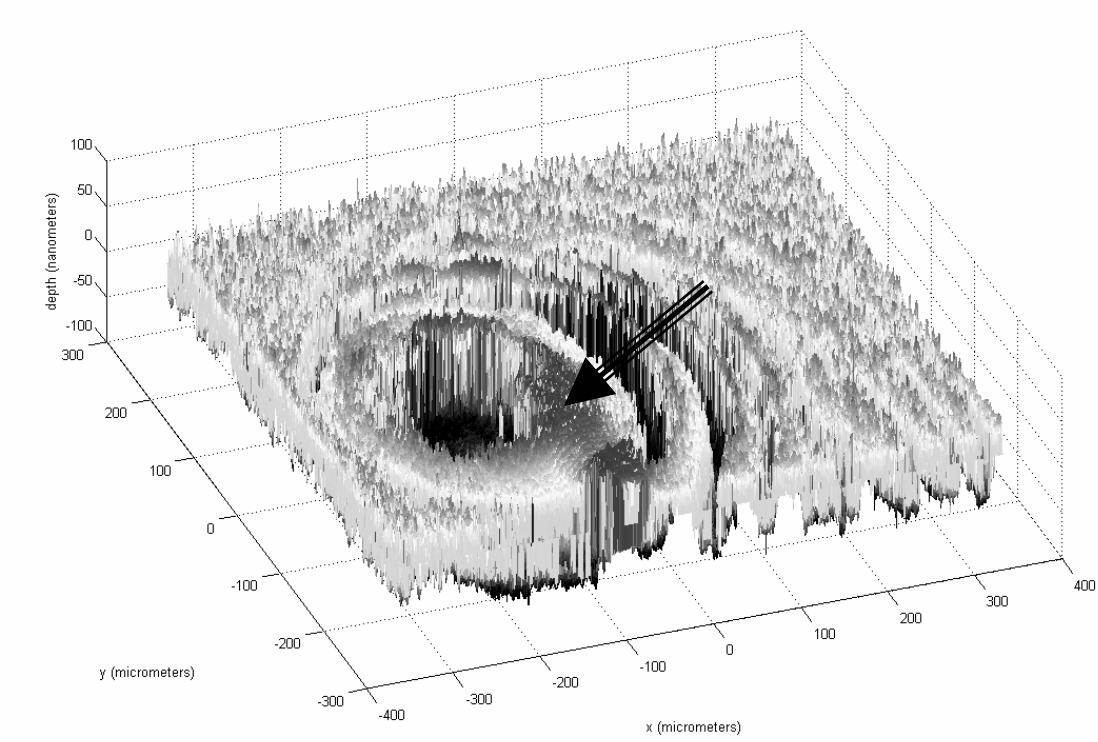

Figure 7 : Interferogram of the metal surface. Axes are x and y in micrometers and z in nanometers.

4. DISCUSSION

Our experiments indicate that the PDI, Point Diffraction Interferometer, concept can be used to make high resolution and high definition topographic maps of metal surfaces. The PDI eliminates is characterized by that the object and reference beams follow the same optical path and therefore eliminates some of the usual problems with interferometers, e.g. noise caused by differential vibrations and short coherence lengths of diode lasers.

The possible resolution in depth is also adequate for most applications. Large areas can be mapped at single imaging with the use of high resolution CCD or CMOS chips. Such chips are under extreme development and chips with 10 million pixels or more are presently available at relatively lo prices. Time will therefore work for our system since the resolution over a certain area in the plane of the surface is directly proportional to the number of available pixels.

The physical size of the imaging chip is also a factor. A large chip, 20 mm or more, is preferable since this will help to aim at the target area. A very small chip may create unwanted interference fringes at the edges. A lens is not necessary on the camera since the observation is in the aperture plane and the PDI image is imaged directly on the chip.

Further development is necessary to reduce the effect of the curved laser beam area. This can be either modeled or measured with a perfectly flat mirror. A useful way we intend to try is to move the object a fraction in one direction along the (x,y)-plane. The pinhole pattern and the beam area curvature will then remain the same, while the object surface pattern will move a fraction. The object surface can then be readily determined from a small number of such translations.

We intend to continue our development of the PDI technology for surface topography. Our next work in the development will be:

1. Refine the pinhole size vs. the transparency.
2. Remove the effect of the laser beam expanded area curvature.
3. Use multiple wavelengths to increase the ambiguity distance.
4. A third wavelength and use of modern phase tracking algorithms will be tried to substantially extend the ambiguity into several hundreds of micrometers.
5. Determine the limitations for techniques for reflectivity and complexity.
6. Measure a large surface by moving the object in the (x,y)-plane.
7. Use a cylindrical lens in the path in order to measure along a curved surface, e.g. the inside of a cylinder.

Our final intent is to create a new instrument technology to measure surfaces with high resolution, high sensitivity and high definition and as a viable on-line and real-time tool in situ in industrial process applications.

5. REFERENCES

[Baath 1991] Baath,L.B.; "A Closer Look at Active Galactic Nuclei: The Great Engines of the Universe"; In: *Physica Scripta, ed. A.Elvius, vol T43* , p57

[Baath et al 1991] Baath,L.B., Padin,S., Woody,D., Rogers,A.E.E., Wright,M.C.H., Zensus,A., Kus,A.J., Backer,D.C., Booth,R.S., Carlstrom,J.E., Dickman,D.C., Emerson,D.T., Hirabyashi,H., Hodges,M.W., Inoue,M., Moran,J.M., Morimoto, M., Payne,J., Plambeck,R.L., Predmore,C.R., and Rönnäng,B.; "The Microarcsecond Structure of 3C273 at 3mm"; In: *Astron. Astroph.*, p. 47

[Baath 1993] Baath,L.B.; "Millimetre VLBI capability status"; In: *Sub-arc second Radio Astronomy, eds. R.J.Davies and R.S.Booth*, p. 431, Cambridge Univ. Press

[Baath 2003] Baath,L.B.; "To See what You cannot See"; In: *SCIA2003 Conference Goteborg, Sweden 2003*

[Bolton and Stanley 1948] Bolton,J.G. and Stanley,G.J.; "Observations on the Variable Source Radio-frequency Radiation in Constellation Cygnus"; In: *Australian J. Sci. Res. Ser. A, vol.1*, p. 58

[Carr et al 1991] Carr,L.W., Chandrasekhara,M.S., and Brock,N.J.; "A Quantitative Study of Unsteady Compressable Flow on an Oscillating Airfoil"; In: *AIAA 22nd Fluid Dynamics, Plasma Dynamics and Laser Conference, Honolulu, Hawai,* p. 58

[Nilsson, Baath and Malmberg 2007] Nilsson,E.J., Baath,L.B., and Malmberg,D.; "Blast Furnace Burden Topography"; In: *Mets & Props 2008 Huddersfield*

[Smartt and Steel Nilsson 1975] Smartt,R.N. and Steel,W.H..; "Theory and applications of Point Diffraction Interferometers"; In: *Japan J. Appl. Physics,* vol 14, Suppl 14-1

[Zensus 1988] Zensus,A.J., Baath,L.B., Cohen,M.H., and Nicholson,G.; "The Inner Radio Jet of 3C273"; In: *Nature*, p. 410